Journal of Nuclear Materials 400 (2010) 151–156

Contents lists available at ScienceDirect

Journal of Nuclear Materials

journal homepage: www.elsevier.com/locate/jnucmat

Optical properties of UO_2 and PuO_2

Hongliang Shi [a,b], Mingfu Chu [c], Ping Zhang [a,d,*]

[a] LCP, Institute of Applied Physics and Computational Mathematics, P.O. Box 8009, Beijing 100088, People's Republic of China
[b] SKLSM, Institute of Semiconductors, Chinese Academy of Sciences, P.O. Box 912, Beijing 100083, People's Republic of China
[c] State Key Laboratory for Surface Physics and Chemistry, Mianyang 621907, People's Republic of China
[d] Center for Applied Physics and Technology, Peking University, Beijing 100871, People's Republic of China

ARTICLE INFO

Article history:
Received 20 November 2009
Accepted 25 February 2010

ABSTRACT

We perform first-principles calculations of electronic structure and optical properties for UO_2 and PuO_2 based on the density functional theory using the generalized gradient approximation (GGA) + *U* scheme. The main features in orbital-resolved partial density of states for occupied *f* and *p* orbitals, unoccupied *d* orbitals, and related gaps are well reproduced compared to experimental observations. Based on the satisfactory ground-state electronic structure calculations, the dynamical dielectric function and related optical spectra, i.e., the reflectivity, adsorption coefficient, energy-loss, and refractive index spectrum, are obtained. These results are consistent with the available experiments.

1. Introduction

Actinide dioxides (AnO_2) have been attracted lots of attention due to their rich physical phenomena characterized by the complex nature of 5*f* electrons. Many experimental and theoretical works have been devoted to investigating the thermodynamical, electronic structural, and defect properties of AnO_2 systems. Taking UO_2 and PuO_2 for example, their insulating ground states have been established experimentally [1,2] and successfully predicted theoretically [3–12]. When referring to insulators or semiconductors, one basic physical quantity of interest is their band-gaps. If the band gap of UO_2 or PuO_2 can be comparable to semiconductors, one idea may occur to us that whether they can be applied extensively in the electronic and optoelectronic devices like semiconductors (Si, GaAs, and ZnO) or not. Recently, Meek et al. discussed the electronic properties of uranium dioxide and revealed the potential performance advantages of uranium dioxide as compared to conventional semiconductor materials [13]. Especially, the higher dielectric constant of UO_2 makes it more suitable for making integrated circuits [13]. This may stimulate many studies of the optical properties for actinide dioxides in future.

Density functional theory (DFT) applied local density approximation (LDA) or GGA usually underestimates band-gaps of semiconductors, which are important for optical spectra. Although an accurate quantitative description of optical spectra requires a treatment beyond the independent particle picture, a qualitative agreement between theory and experiment can often be obtained on the level of DFT [14]. Optical adsorption and reflectance spectra of semiconductors have been studied for several decades both experimentally and theoretically, whereas, similar works performed on actinide dioxides is still very scarce although they are necessary not only from the viewpoint of basic science but also from their technological importance in industries. Experimentally, Schoenes studied the incidence reflectivity of UO_2 single crystals in the photon energy range of 0.03–13 eV, from which the complex dielectric function $\varepsilon(\omega) = \varepsilon_1(\omega) + i\varepsilon_2(\omega)$ has been derived [15]. For PuO_2, to our knowledge, no experimental optical data are available in the literature. As for the theoretical investigations of optical spectrum of actinide dioxides, it is a great challenge to standard density functional theory that an accurate description of electronic structure for actinide oxides is hard to be achieved, which is indispensable to getting the correct optical spectrum. Conventional density functional schemes that apply LDA or the GGA underestimate the strong on-site Coulomb repulsion of the 5*f* electrons and consequently fail to capture the correlation-driven localization and even predict actinide oxides to be uncorrect ground states. Therefore, the 5*f* electrons in actinide oxides require special attention. One promising way to improve contemporary LDA and GGA approaches is to modify the intra-atomic Coulomb interaction through the so-called LDA + *U* or GGA + *U* approach, in which the underestimation of the intraband Coulomb interaction is corrected by the Hubbard *U* parameter [16,17]. Recently, the electronic structures of UO_2 and PuO_2 are correctly reproduced using LDA + *U* or GGA + *U* calculations [3–11]. Therefore, based on the good performance of LDA/GGA + *U* approaches in describing the electronic structure of the systems containing 5*f* electrons, it is encouraging to investigate the optical spectra of them.

* Corresponding author at: LCP, Institute of Applied Physics and Computational Mathematics, P.O. Box 8009, Beijing 100088, People's Republic of China. Tel.: +86 10 62014411 2208.
E-mail address: zhang_ping@iapcm.ac.cn (P. Zhang).

0022-3115/$ - see front matter © 2010 Elsevier B.V. All rights reserved.
doi:10.1016/j.jnucmat.2010.02.024

In this work, we used the GGA + U scheme to study the static and frequency-dependent dynamical dielectric response functions for UO_2 and PuO_2. Our present calculated band gap E_g and high-frequency dielectric constant ε_∞ for UO_2 are 2.3 eV and 5.53, which are in good agreement with the experimental values of about 2.1 eV and 5.1 observed in the optical spectra [15], respectively. Furthermore, our calculated dielectric function $\varepsilon(\omega)$ exhibits the overall agreement with experimental result and the main peaks are well reproduced. The dielectric function and the consequent optical spectra for PuO_2 are also calculated in the paper. In particular, the value of ε_∞ for PuO_2 is predicted to be 6.21, a little larger than that for UO_2. Considering the satisfactory calculations for UO_2, we expect our predicted optical behavior for PuO_2 can provide a useful reference for future experimental measurement.

2. Details of calculation

Our electronic structural and optical calculations are performed using the projector-augmented wave (PAW) method of Blöchl [18], as implemented in the ab initio total-energy and molecular-dynamics program Vienna *ab initio* simulation program (VASP) [19]. PAW is an all-electron method that combines the accuracy of augmented-plane-wave methods with the efficiency of the pseudopotential approach. The PAW method is implemented in VASP with the frozen-core approximation. The exchange-correlation functional is used GGA of Perdew–Burke–Ernzerhof (PBE) formalism [20]. The 5*f*, 6*s*, 6*p*, 6*d* and 7*s* electrons of U and Pu as well as the oxygen 2*s* and 2*p* electrons are explicitly treated as valence electrons. The electron wave function is expanded in plane waves up to a cutoff energy of 500 eV. For the Brillouin zone integration, the Γ centered $6 \times 6 \times 6$ grid is adopted. 144 bands are used to get the dynamical dielectric function $\varepsilon(\omega)$ and a good convergence can be achieved. In order to perform the antiferromagnetic (AFM) phase calculations, we used the unit cell containing 12 atoms. The strong on-site Coulomb repulsion among the localized 5*f* electrons is described by using the formalism formulated by Dudarev et al. [21]. In this scheme, only the difference between the spherically averaged screened Coulomb energy U and the exchange energy J is important for the total LDA (GGA) energy functional. Thus, in the following we label them as one single effective parameter U for brevity. In our calculation, we use $J = 0.51$ and 0.75 eV for the exchange energies of U and Pu, respectively, and the effective Hubbard U are 4.0 and 3 eV, which are close to the values used in other previous work [4,5].

For the subtle AFM order of UO_2 and PuO_2, we used the simple layered AFM structure [9] instead of the non-collinear AFM structure [22]. In our work, the Pu and U spin magnetic moments are confined along the *z*-axis in a simple +−+− alternation of spins. Notice that in our calculations optimized lattice constants of 5.550 and 5.462 Å for UO_2 and PuO_2 are used, respectively, which are obtained by fitting the third-order Birch–Murnaghan equation of state (EOS) [23]. In our calculations, the structures are not relaxed and all the atoms are fixed in their ideal positions in CaF_2-type structure. Therefore, the distortion in the structure of UO_2 with a collinear AFM order [6,8] is not taken into account. we also choose several different initial magnetic moments for Pu and U ions, and find the total energies and magnetic moments are rapidly converged to the same results, respectively. Therefore, the correct ground state is obtained avoiding metastable states [8,11,24].

As for the optical spectra calculations, we adopt two different methods to determine the macroscopic static dielectric constants using different approximations [14]. One method is using a summation over conduction band states and the other is using the linear response theory (density functional theory). For the latter, only the static ion-clamped dielectric matrix can be obtained and a summation over empty conduction band states is not required, whereas the former can calculate the frequency-dependent dynamic dielectric function after the electronic ground state has been obtained. The frequency-dependent imaginary part of the dielectric function is determined by a summation over empty states using the following equation [14]:

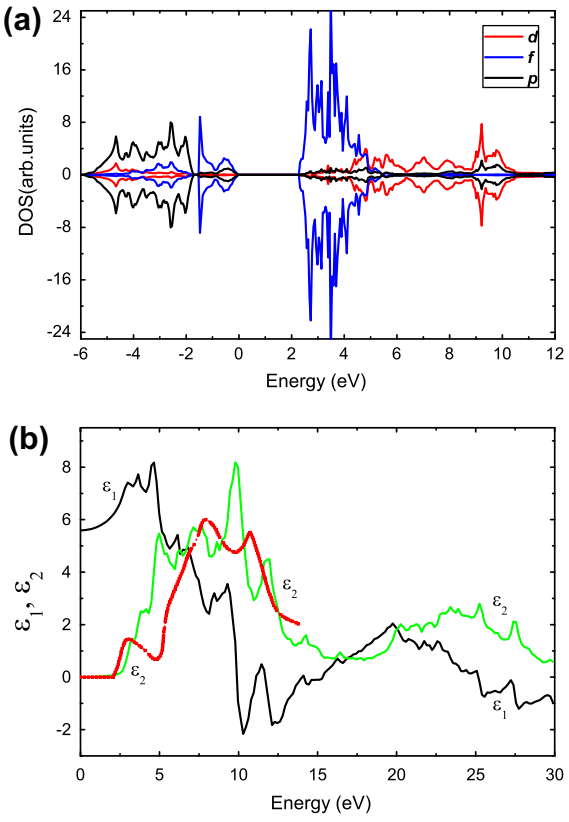

Fig. 1. (a) The projected orbital-resolved partial DOS for U 6*d*, U 5*f*, and O 2*p* orbitals in antiferromagnetic UO_2. The Fermi level is set to zero. (b) The dynamical dielectric function $\varepsilon(\omega) = \varepsilon_1(\omega) + i\varepsilon_2(\omega)$ as a function of the photon energy ω for UO_2. The black and green lines represent our calculated real and imaginary parts of dielectric function $\varepsilon(\omega)$, respectively, while the red dotted-line is experimental $\varepsilon_2(\omega)$. (For interpretation of the references to color in this figure legend, the reader is referred to the web version of this article.)

Table 1
Ion clamped static macroscopic dielectric constants ε_∞ of UO_2 and PuO_2 calculated using the PAW method and various approximations with various *k*-points sampling: Γ indicates a grid centered at Γ point, whereas Monkhorst–Pack (MP) grids do not contain the Γ point. N_k stands the number of irreducible *k*-points of the Brillouin zone (IBZ) at specific *k*-points sampling. ε_{mic} indicates values neglecting local field effects, ε_{RPA} includes local fields effects in the Hartree approximation, and ε_{DFT} includes local fields effects on the DFT level. ε^{cond} are values obtained by summation over conduction band states, whereas ε^{LR} are values obtained using linear response theory (density functional perturbation theory).

AnO_2	*k*-mesh	N_k(IBZ)	ε^{LR}_{mic}	ε^{LR}_{RPA}	ε^{LR}_{DFT}	ε^{cond}_{mic}
UO_2	$(12 \times 12 \times 12)$ Γ	196	5.71	5.28	5.53	5.59
	$(8 \times 8 \times 8)$ Γ	75	5.71	5.28	5.53	5.59
	$(6 \times 6 \times 6)$ Γ	40	5.71	5.28	5.53	5.59
	$(6 \times 6 \times 6)$ MP	18	5.71	5.28	5.53	5.59
PuO_2	$(12 \times 12 \times 12)$ Γ	196	6.38	5.94	6.21	6.23
	$(8 \times 8 \times 8)$ Γ	75	6.37	5.94	6.20	6.23
	$(6 \times 6 \times 6)$ Γ	40	6.37	5.94	6.21	6.23
	$(6 \times 6 \times 6)$ MP	18	6.37	5.94	6.20	6.23

$$\varepsilon^{(2)}_{\alpha\beta}(\omega) = \frac{4\pi^2 e^2}{\Omega} \lim_{q\to 0} \frac{1}{q^2} \sum_{c,v,\mathbf{k}} 2w_{\mathbf{k}} \delta(\varepsilon_{c\mathbf{k}} - \varepsilon_{v\mathbf{k}} - \omega) \times \left\langle u_{c\mathbf{k}+\mathbf{e}_\alpha \mathbf{q}} | u_{vk} \right\rangle \left\langle u_{c\mathbf{k}+\mathbf{e}_\beta \mathbf{q}} | u_{v\mathbf{k}} \right\rangle^*, \quad (1)$$

where the indices c and v refer to conduction and valence band states respectively, and $u_{c\mathbf{k}}$ is the cell periodic part of the wavefunctions at the k-point $\mathbf{k}$. The real part of the dielectric tensor is obtained by the usual Kramers–Kronig transformation

$$\varepsilon^{(1)}_{\alpha\beta}(\omega) = 1 + \frac{2}{\pi} P \int_0^\infty \frac{\varepsilon^{(2)}_{\alpha\beta}(\omega')\omega'}{\omega'^2 - \omega^2 + i\eta} d\omega', \quad (2)$$

where P denotes the principal value.

The main optical spectra, such as the reflectivity $R(\omega)$, adsorption coefficient $I(\omega)$, energy-loss spectrum $L(\omega)$, and refractive index $n(\omega)$, all can be obtained from the dynamical dielectric response functions $\varepsilon(\omega)$. The explicit expressions are given by

$$R(\omega) = \left| \frac{\sqrt{\varepsilon(\omega)} - 1}{\sqrt{\varepsilon(\omega)} + 1} \right|^2, \quad (3)$$

$$I(\omega) = (\sqrt{2})\omega \left[\sqrt{\varepsilon_1(\omega)^2 + \varepsilon_2(\omega)^2} - \varepsilon_1(\omega) \right]^{1/2}, \quad (4)$$

$$L(\omega) = \varepsilon_2(\omega) / \left[\varepsilon_1(\omega)^2 + \varepsilon_2(\omega)^2 \right], \quad (5)$$

and

$$n(\omega) = (1/\sqrt{2}) \left[\sqrt{\varepsilon_1(\omega)^2 + \varepsilon_2(\omega)^2} + \varepsilon_1(\omega) \right]^{1/2}, \quad (6)$$

respectively.

3. Results and discussion

3.1. Electronic structure and optical properties of UO_2

Since the optical spectra are directly calculated from interband transitions, an accurate description of the electronic structure is indispensable. The calculated orbital-resolved partial density of states (PDOS) for U 5*f*, U 6*d* and O 2*p* are shown in Fig. 1a. The Fermi level is set to be zero. It is clearly shown that the valence bands are mainly contributed by U 5*f* and O 2*p* orbitals. The peak near the Fermi level is mainly U 5*f* with a little O 2*p* contribution, which bas been confirmed by the resonant photoemission [25]. The U 5*f* valence band covers from 0 to −1.6 eV, which is also consistent with the experimental observation that the occupied 5*f* states in UO_2 are located around 1.5 eV below the Fermi level with a band width of about 2.0 eV [25]. The O 2*p* valence band width is 4.0 eV from about −1.8 to −5.8 eV, in qualitative agreement with the photoemission value of 5.0 eV from −3.0 to −8.0 eV [25].

As for the unoccupied U 5*f* and 6*d* orbitals, their accurate descriptions are also indispensable to the interband transitions, since electrons are excited from the occupied valence bands to the unoccupied bands during optical excitations. The 5*f* and 6*d* bands begin at about 2.3 and 4 eV, respectively, which are well consistent with the results of 2.6 and 5 eV obtained by hybrid DFT method [26]. Note that our calculated $p \rightarrow d$ gap is 5.8 eV, which accords well with the Bremsstrahlung Isochromat Spectroscopy (BIS) value of 5.0 ± 0.4 eV [27]. Overall, our calculated DOS agrees well the experimental spectra and other theoretical results. This supplies the safeguard for our following optical spectrum calculations.

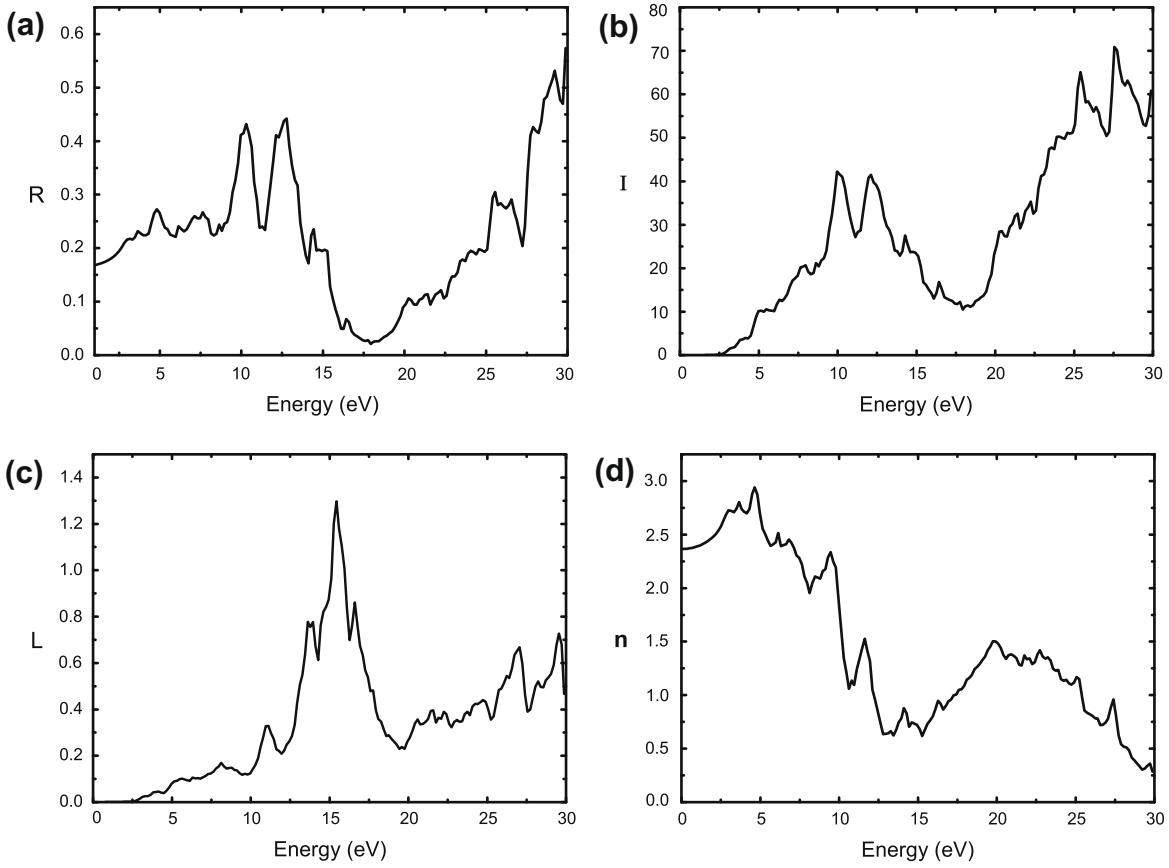

Fig. 2. Calculated optical spectra for UO_2, (a) the reflectivity $R(\omega)$, (b) adsorption coefficient $I(\omega)$, (c) energy-loss $L(\omega)$, and (d) refractive index $n(\omega)$.

Due to the cubic symmetry of UO_2, the dielectric tensor only has one independent component and $\varepsilon_{xx} = \varepsilon_{yy} = \varepsilon_{zz}$. Our calculated macroscopic dielectric constants ε_∞ using different methods and approximations are collected in Table 1. We find that well converged results can be obtained by using the Γ-centered $6 \times 6 \times 6$ grid. Note that the value of ε_{DFT}^{LR} should be compared to experiment. For UO_2, the calculated ε_∞ is 5.53, which agrees well with the experimental value of 5.1 [15].

As for the dynamical dielectric function, our calculated imaginary part $\varepsilon_2(\omega)$ and real part $\varepsilon_1(\omega)$ of the complex dielectric function $\varepsilon(\omega)$ together with the corresponding experimental $\varepsilon_2(\omega)$ are showed in Fig. 1b. The green and black lines represent our calculated imaginary and real parts of the complex dielectric function $\varepsilon(\omega)$, respectively, while the red dotted-line gives the experimental measurement [15] of $\varepsilon_2(\omega)$. Our theoretical photon energy covers from 0 to 30 eV, while the experimental [15] value covers from 0 to 13 eV. According to our calculated DOS showed in Fig. 1a, we suggest that in $\varepsilon_2(\omega)$ the peaks (at 2.8 eV) below 3 eV should be assigned to the intra 5*f* transitions. Notice that the unoccupied 6*d* bands begin about at 4 eV, therefore, the $5f \rightarrow 6d$ transition energies should be larger than 4 eV. Kudin et al. also suggested that the stronger adsorption observed experimentally at ~5–6 eV could be assigned to the optically allowed $5f \rightarrow 6d$ transitions [26]. According to our calculated $\varepsilon_2(\omega)$, four main peaks lie at about 5.0, 7.1, 9.8, and 11.8 eV, respectively. The shape of the calculated curve exhibits the same main features demonstrated by the experimental results [15]. Combined with the orbital-resolved PDOS shown in Fig. 1a, we attribute the first two peaks in $\varepsilon_2(\omega)$ to be $5f \rightarrow 6d$ transitions, while the last two to be $2p \rightarrow 6d$ transitions. This is well consistent with the experimental assignment [28] by Naegele et al., who attributed the peak around 3 eV in $\varepsilon_2(\omega)$ to intra $5f^2$ transitions, while the peak structures above 5 and 10 eV were ascribed to the $f \rightarrow d$ and $p \rightarrow d$ transitions, respectively. Another assignment was suggested by Schoenes according to their dielectric function deduced from the reflectivity measurement; they argued that the peaks near 3 and 6 eV correspond to $f \rightarrow d$ transitions, and that the peaks near 8 and 11 eV are due to $p \rightarrow d$ transitions [15,29]. Herein, the assignment of $f \rightarrow d$ transition at 3 eV in Refs. [15,29] is not supported by our calculation. The cause is that in assigning the peak in $\varepsilon_2(\omega)$ at 3 eV, the energy distance between U occupied $5f^2$ and O 2*p* valence bands was overestimated in Refs. [15,29] to be as large as 4 eV, which is much larger than that directly determined by the photoemission measurements [25,30,31]. On the contrary, according to our band-structure calculation, the occupied 5*f* orbitals are locate at about 1.5 eV below the Fermi level and the O 2*p* bands widely covers from about −1.8 to −5.8 eV, which instead accords well with the experimental photoemission data [25,30,31] in UO_2. Thus, as mentioned above, we suggest the structure in $\varepsilon_2(\omega)$ below 3 eV is caused by the intra 5*f* transitions.

Using expressions (3)–(6), the reflectivity $R(\omega)$, adsorption coefficient $I(\omega)$, energy-loss $L(\omega)$ and refractive index $n(\omega)$ spectra are showed in Fig. 2. For reflectivity $R(\omega)$ spectrum, there are four peaks located at 4.8, 7.6, 10.3, and 12.8 eV. The adsorption coefficient $I(\omega)$ spectrum has the same trends. The origin of these peaks can also be explained as the peaks of the imaginary part $\varepsilon_2(\omega)$. Note that three similar peaks at 5.5, 8, 11.7 eV are also observed by the reflectance spectrum up to 13 eV at room temperature for UO_2 [15]. The energy-loss $L(\omega)$ spectrum can demonstrate not only one-particle excitations but also collective excitations. The maxima at around 15.4 eV as showed in Fig. 2c indicates the plasmon resonance, which is qualitatively consistent with the experimental value of 14 eV [29]. As showed in Fig. 1b, at about 11.7 eV the real part ε_1 becomes zero, arriving at the minima around 12.1 eV and then approaches zero at about 14 eV. As Schoenes pointed out, the energy at which $\varepsilon_1(\omega)$ crosses the zero line with a positive slop gives the plasmon excitation energy [29].

3.2. Electronic structure and optical properties of PuO_2

Due to Pu unique position of its 5*f* electrons between localized and delocalized states in the actinide series, Pu metal and plutonium-based oxides have more complex properties than other actinides. For example, metallic Pu has six different phase under different temperatures and pressures [32]. PuO_2 as an important actinide dioxide has extensive applications in nuclear reactor fuel and long-term storage of surplus plutonium. Therefore, the study of optical properties for PuO_2 is also necessary and interesting. However, no experimental results of optical properties for PuO_2 in the literature are available. Recently, Butterfield et al. studied the photoemission behavior of surface oxides of δ-plutonium and they observed that two peaks characterized by Pu 5*f* and O 2*p* orbitals are dominant in PuO_2 and Pu_2O_3 [33]. For PuO_2, the two peaks observed are located at approximately 2.5 and 4.6 eV [33], and our calculated DOS showed in Fig. 3a also present two similar peaks, i.e., a strong peak at about 1.6 eV and a weaker one at 3.7 eV. Overall, these features are well reflected in our PDOS showed in Fig. 3a compared to experimental observations. As for the unoccupied 6*d* states, no experimental data can be obtained. Our calculated unoccupied 6*d* states begin at about 5 eV. Considering the O 2*p* peak at −3.7 eV, we suggest the $p \rightarrow d$ transitions occur at larger energies than 9 eV.

Our calculated macroscopic dielectric constant ε_∞ for PuO_2 are also collected in Table 1. The present ε_∞ is 6.21, whereas, no exper-

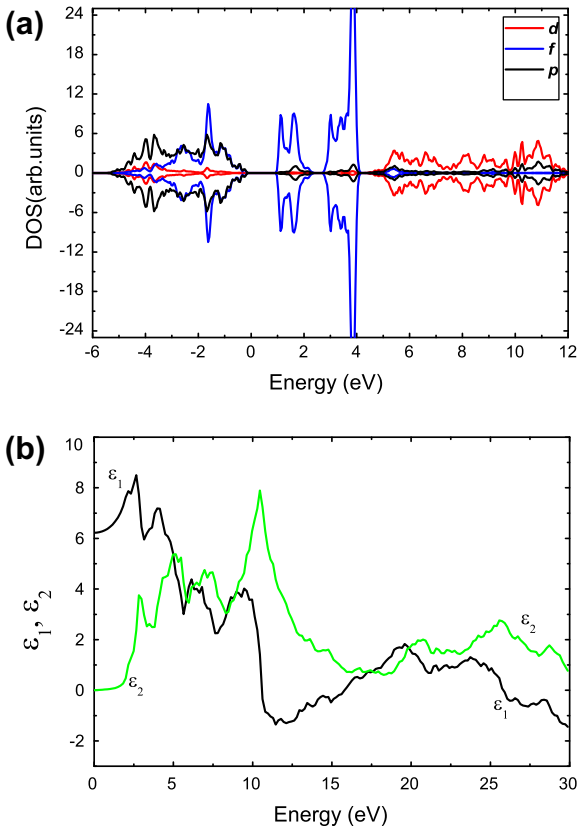

Fig. 3. (a) The projected orbital-resolved partial DOS for Pu 6*d*, Pu 5*f*, and O 2*p* orbitals in antiferromagnetic PuO_2. The Fermi level is set to zero. (b) The dynamical dielectric function $\varepsilon(\omega) = \varepsilon_1(\omega) + i\varepsilon_2(\omega)$ as a function of the photon energy ω for PuO_2. The black and green lines represent our calculated real and imaginary parts of dielectric function $\varepsilon(\omega)$, respectively. (For interpretation of the references to color in this figure legend, the reader is referred to the web version of this article.)

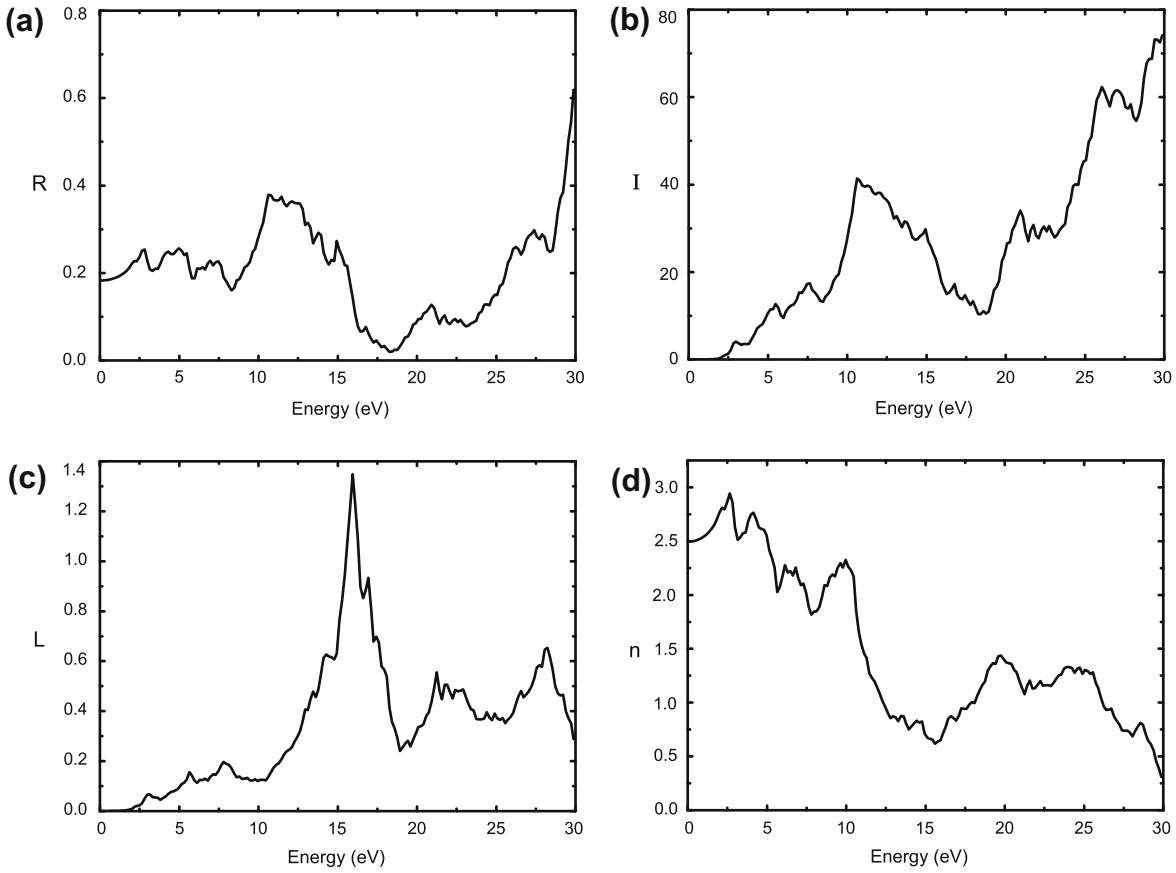

Fig. 4. Calculated optical spectra for PuO_2, (a) the reflectivity $R(\omega)$, (b) adsorption coefficient $I(\omega)$, (c) energy-loss $L(\omega)$, and (d) refractive index$n(\omega)$.

imental value is available at present. Our calculated imaginary part $\varepsilon_2(\omega)$ and real part $\varepsilon_1(\omega)$ of the complex dielectric function $\varepsilon(\omega)$ are showed in Fig. 3b. For $\varepsilon_2(\omega)$, four main peaks locate at 2.8, 5.1, 7.5, and 10.5 eV. According to our PDOS calculation showed in Fig. 3a, we attribute the peak below 6 eV to be intra 5*f* transitions, and the last two to be $f \rightarrow d$ and $p \rightarrow d$ transitions, respectively. The two similar peaks at 7 and 10 eV are also obtained by Jomard et al. using *ab initio* calculations [11].

Other related optical spectra for PuO_2 are showed in Fig. 4. For reflectivity $R(\omega)$ spectrum, there are four peaks at 2.8, 5.0, 7.5, and 10.6 eV. Similarly, four peaks at 3.0, 5.5, 7.6, 10.6 eV are also observed in the adsorption coefficient $I(\omega)$ spectrum. The origin of these peaks can also be explained according to the structure displayed in the imaginary part $\varepsilon_2(\omega)$ of the dielectric function. It is evident that the plasmon excitation occurs at 16.0 eV, which is similar to the case of UO_2 at 15.4 eV as mentioned above.

4. Summary

In summary, we have performed a detailed investigation of the electronic structure and optical spectra of actinide dioxides UO_2 and PuO_2 using first-principles methods. For UO_2, our calculated projected orbital-resolved PDOS for U 5*f* and O 2*p* orbitals in the valence region agree well with the experimental photoemission observation. As for the unoccupied states, our calculated *p–d* gap is 5.8 eV, similar to the experimental BIS value of 5.0 ± 0.4 eV. The calculated insulating band gap E_g and macroscopic static dielectric constants ε_∞ for UO_2 are 2.3 eV and 5.53, respectively, which are also in good agreement with the experimental values of about 2.1 eV and 5.1. The main features in spectra for UO_2 are also well reproduced by our calculated dynamical dielectric function $\varepsilon(\omega)$ compared to the experimental observation. For PuO_2, the two main peaks characterized by Pu 5*f* and O 2*p* orbitals in valence bands are evidenced in our calculated PDOS, which accords well with the photoemission results. The calculated macroscopic static dielectric constants ε_∞ is 6.21. The related optical spectra for PuO_2 are also obtained by calculating the dynamical dielectric function. The $f \rightarrow d$ and $p \rightarrow d$ transitions are found to occur at 7.5 and 10.5 eV, respectively. Considering the satisfactory optical description for UO_2 compared to experiments, we expect that these results for PuO_2 are also reasonable and therefore can provide a useful reference for future experimental measurement.

Acknowledgement

This work was supported by the Foundations for Development of Science and Technology of China Academy of Engineering Physics under Grant No. 2009B0301037.

References

[1] J. Faber Jr., G.H. Lander, B.R. Cooper, Phys. Rev. Lett. 35 (1975) 1770.
[2] C.E. McNeilly, J. Nucl. Mater. 11 (1964) 53.
[3] H. Geng, Y. Chen, Y. Kaneta, M. Kinoshita, Phys. Rev. B 77 (2008) 180101.
[4] B. Sun, P. Zhang, X.-G. Zhao, J. Chem. Phys. 128 (2008) 084705.
[5] D.A. Andersson, J. Lezama, B.P. Uberuaga, C. Deo, S.D. Conradson, Phys. Rev. B 79 (2009) 024110.
[6] M. Iwasawa, Y. Chen, Y. Kaneta, T. Ohnuma, H.-Y. Geng, M. Kinoshita, Mater. Trans. 47 (2006) 2651.
[7] P. Nerikar, T. Watanabe, J.S. Tulenko, S.R. Phillpot, S.B. Sinnott, J. Nucl. Mater. 384 (2009) 61.
[8] B. Dorado, B. Amadon, M. Freyss, M. Bertolus, Phys. Rev. B 79 (2009) 235125.
[9] F. Gupta, G. Brillant, A. Pasturel, Philos. Mag. 87 (2007) 2561.
[10] D. Gryaznov, E. Heifets, E. Kotomin, Phys. Chem. Chem. Phys. 11 (2009) 7241.
[11] G. Jomard, B. Amadon, F. Bottin, M. Torrent, Phys. Rev. B 78 (2008) 075125.

[12] L. Petit, A. Svane, Z. Szotek, W.M. Temmerman, G.M. Stocks, Phys. Rev. B 81 (2010) 045108.
[13] T. Meek, M. Hu, M. Haire, <http://www.nuenergy.org/pdf/UO2semicond.pdf>.
[14] M. Gajdoš, K. Hummer, G. Kresse, J. Furthmüller, F. Bechstedt, Phys. Rev. B 73 (2006) 045112.
[15] J. Schoenes, J. Appl. Phys. 49 (1978) 1463.
[16] V.I. Anisimov, I.V. Solovyev, M.A. Korotin, M.T. Czyżyk, G.A. Sawatzky, Phys. Rev. B 48 (1993) 16929.
[17] I.V. Solovyev, P.H. Dederichs, V.I. Anisimov, Phys. Rev. B 50 (1994) 16861.
[18] P.E. Blöchl, Phys. Rev. B 50 (1994) 17953.
[19] G. Kresse, J. Hafner, Phys. Rev. B 48 (1993) 13115.
[20] J.P. Perdew, K. Burke, M. Ernzerhof, Phys. Rev. Lett. 77 (1996) 3865.
[21] S.L. Dudarev, G.A. Botton, S.Y. Savrasov, C.J. Humphreys, A.P. Sutton, Phys. Rev. B 57 (1998) 1505.
[22] R. Caciuffo, G. Amoretti, P. Santini, G.H. Lander, J. Kulda, P.deV. Du Plessis, Phys. Rev. B 59 (1999) 13892.
[23] F. Birch, Phys. Rev. 71 (1947) 809.
[24] A.B. Shick, W.E. Pickett, A.I. Liechtenstein, J. Electron Spectrosc. Related Phenomena 114 (2001) 753.
[25] L.E. Cox, W.P. Ellis, R.D. Cowan, J.W. Allen, S.-J. Oh, I. Lindau, B.B. Pate, A.J. Arko, Phys. Rev. B 35 (1987) 5761.
[26] K.N. Kudin, G.E. Scuseria, R.L. Martin, Phys. Rev. Lett. 89 (2002) 266402.
[27] Y. Baer, J. Schoenes, Solid State Commun. 33 (1980) 885.
[28] J. Naegele, L. Manes, U. Birkholz, in: H. Blank, R. Lidner (Eds.), Proc. 5th Int. Conf. Plutonium and other Actinides, North-Holland, Amsterdam, 1976, p. 393.
[29] J. Schoenes, Phys. Rep. 63 (1980) 301.
[30] J. Naegele, J. de Phys. C4 (1979) 169.
[31] P.R. Norton, R.L. Tapping, D.K. Creber, W.J.L. Buyers, Phys. Rev. B 21 (1980) 2572.
[32] K.T. Moore, G. van der Laan, Rev. Mod. Phys. 81 (2009) 235.
[33] M. Butterfield, T. Durakiewicz, E. Guziewicz, J. Joyce, A. Arko, K. Graham, D. Moore, L. Morales, Surf. Sci. 571 (2004) 74.